

# Light propagation in clouds and snowfall for earth-based sources (results of Monte Carlo simulation)

S.M. Prigarin and E.A. Belous

*Institute of Computational Mathematics and Mathematical Geophysics,  
Siberian Branch of the Russian Academy of Sciences, Novosibirsk*

Received September 7, 2000

In this paper we present results of numerical modeling of radiation transfer in clouds and snowfall for stationary earth-based light sources. We study the following effects caused by multiple light reflection between Earth's surface and atmosphere with clouds and snowfall: an increase in the range of propagation for a point source and a possible intensification of the luminous flux near the surface.

## 1. Model with a surface-based source

Let us consider the following model. We assume that the underlying surface is a homogeneous Lambertian source of unit power. A photon emitted by the surface can either be absorbed in the atmospheric layer with probability  $P$ , or fly out of the atmospheric layer with probability  $A$ , or return to the underlying surface after scattering in the atmospheric layer with probability  $B = 1 - P - A$ . In the last case the photon either is absorbed by the surface with probability  $R$  or is reflected from the surface with probability  $Q = 1 - R$  according to Lambert's law.

Thus, multiple re-reflections of photons are possible between the atmospheric layer and the underlying surface. The greater is the probability  $B$  of the photon returning to the underlying surface and the greater is the surface albedo  $Q$ , the more significant is the multiple scattering fraction of the re-reflected radiation. If  $\Phi_0$  is the power of the flux emitted by the surface source (i.e., the flux emitted by a surface element of unit area of the underlying surface per unit time interval), the power of the downwelling flux incident on a surface element of unit area of the underlying surface is given by the formula

$$\Phi_1 = \Phi_0 B / (1 - QB).$$

We call the coefficient  $c_\Phi = \Phi_1 / \Phi_0 = B / (1 - QB)$  the flux amplification coefficient (also known as the radiation amplification factor) (in other words,  $c_\Phi$  is nothing other than the mean number of collisions of a given photon with the surface). In addition, we consider the quantity

$$c_\perp = \frac{3}{2} \int_0^1 2\pi I_1(\mu) \mu d\mu,$$

where  $I_1(\mu)$  is the intensity of the radiation returning from the atmospheric layer to the underlying surface expressed as a function of the cosine  $\mu \in [0, 1]$  of the

angle between the direction of the radiant flux and the normal to the surface

$$2\pi \int_0^1 I_1(\mu) \mu d\mu = 1.$$

The value  $c_\perp$  reflects the degree of concentration of the radiation incident on the surface in the direction perpendicular to the surface. Formally, this value can lie in the interval from 0 to  $3/2$  (the extreme value  $3/2$  corresponds to the case where the radiation returning from the atmospheric layer is incident on the surface exactly perpendicularly), but in fact the value of  $c_\perp$  turned out to be less than unity in the calculations presented below. For a Lambertian distribution of the incident radiation  $I_1(\mu) = \mu/\pi$  and  $c_\perp = 1$ .

Note that the illumination of the underlying surface in the considered plane-parallel model with an infinitely extended homogeneous surface-based source is equal to  $\Phi_1$  and does not depend on the directional diagram of the radiation returning to the surface.

The calculations presented in this paper were carried out for an atmosphere with cloud layer and snowfall. It was assumed that clouds and the under-cloud layer with snowfall are homogeneous, uniformly scattering media (the latter assumption is reasonable for the visible wavelength range) with scattering coefficients  $\sigma_{CL}$  and  $\sigma_{SN}$ , respectively.

We denote the distance from the surface to the lower boundary of cloudiness as  $h$  and the height of the cloud layer as  $H$ . Interaction of the radiation with other components of the atmosphere was not taken into account. The  $C_1$  cloud model<sup>1</sup> for optical radiation with wavelength  $\lambda = 0.6 \mu\text{m}$  (mean cosine of the scattering angle 0.86) was used as the scattering phase function in the cloud layer.

The same simplified model as in Ref. 2 was used as the scattering phase function of the snowfall: isotropic scattering with probability 0.5 (corresponding to refraction and reflection of the beam at the boundary

of a randomly oriented snowflake), and uniform scattering with probability 0.5 within a small cone with axis coincident with the forward direction. (This approximation corresponds to diffraction, or small-angle scattering, on a snowflake.)

The maximum scattering angle  $\theta$  in the cone depends on the characteristic snowflake diameter  $d$  and the wavelength  $\lambda$  as follows:  $\theta = \lambda/d$  (for example, for  $d = 1$  mm and  $\lambda = 0.6$   $\mu\text{m}$  we obtain  $\theta = 0.6 \cdot 10^{-3}$  rad). According to the experimental data, snowfalls divide into three types depending on the characteristic snowflake size<sup>3</sup>: snowfalls with small ( $d \approx 1$  mm), intermediate ( $d \approx 4$  mm), and large ( $d \approx 7$  mm) diameter snowflakes. The characteristic values of the extinction coefficient  $\sigma_{\text{SN}}$  in a snowfall can reach  $10^{-2}$   $\text{m}^{-1}$  depending on the number density and size of the snowflakes.

Results of modeling for  $d = 4$  mm and  $\sigma_{\text{CL}} = 20$   $\text{km}^{-1}$  are presented below.

The flux amplification coefficient is plotted in Fig. 1 as a function of the underlying surface albedo. As can be seen from these results, multiple re-reflection

of radiation between the underlying surface and the atmospheric layer with cloudiness and snowfall can lead to an amplification of the radiation flux near the underlying surface by a factor of several-fold. In particular, an almost sixfold increase of the radiation flux was observed in the numerical experiment for certain values of the parameters (see Fig. 1a).

The directional diagram of the radiation returning from the atmospheric layer to the underlying surface and the quantity  $c_{\perp}$  depend significantly on the optical thickness of the layer (Fig. 2). The directional diagram is close to linear for sufficiently great optical thickness, in agreement with Lambert's law.

Examples of dependences of the fraction of radiation absorbed by the underlying surface as well as mean photon trajectory lengths (before the photon has escaped from the upper boundary of cloudiness or has been absorbed by the underlying surface) are shown in Figs. 3 and 4. The convexity of the plots of the fraction of the absorbed radiation is explained by multiple re-reflection of radiation between the underlying surface and the atmospheric layer.

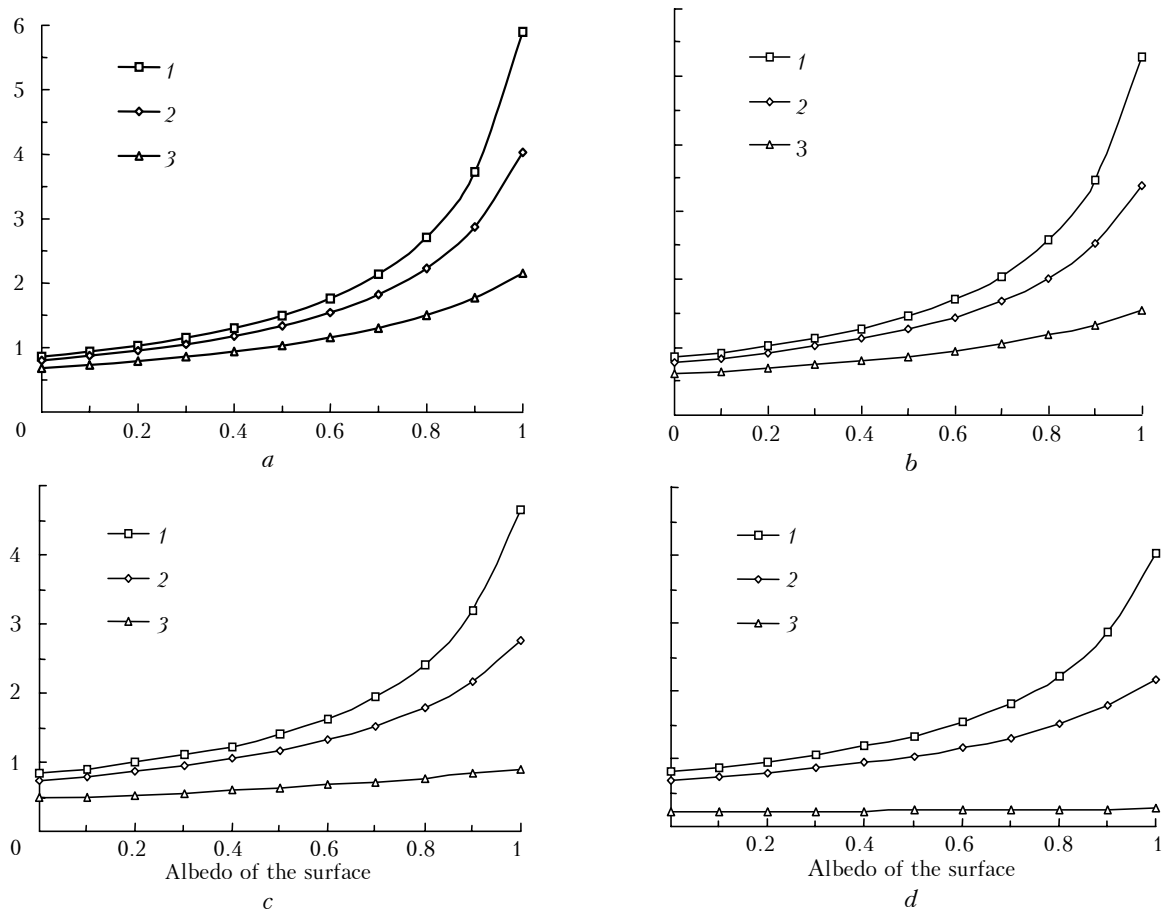


**Fig. 1.** The flux amplification coefficient  $c_{\Phi}$  (mean number of photon collisions with the surface) as a function of the albedo of the underlying surface  $Q$  for different values of the scattering coefficient in snowfall  $\sigma_{\text{SN}}$  and the height of the cloudy layer  $H$ :  $\sigma_{\text{SN}} = 10$  (1); 5 (2); 0  $\text{km}^{-1}$  (3) and  $H = 1$  (a); 0.7 (b); 0.4 (c); 0.1 km (d).

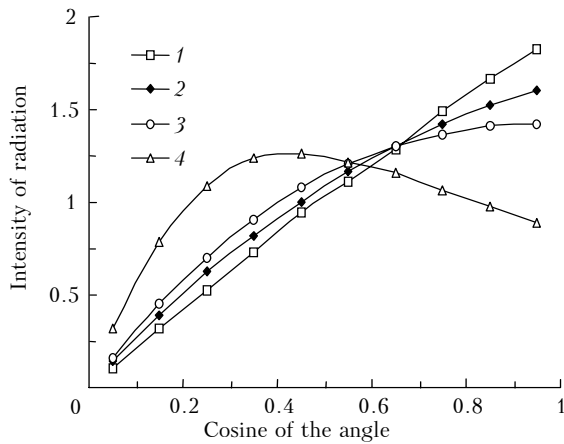


**Fig. 2.** Directional diagram of radiation returning from the atmospheric layer to the underlying surface for  $H = 1$  km and  $\sigma_{SN} = 10 \text{ km}^{-1}$  (1),  $H = 0.7$  km and  $\sigma_{SN} = 0 \text{ km}^{-1}$  (2);  $H = 0.4$  km and  $\sigma_{SN} = 0 \text{ km}^{-1}$  (3);  $H = 0.1$  km and  $\sigma_{SN} = 0 \text{ km}^{-1}$  (4). The dependence presented here is that of the radiation intensity on the cosine of the angle between the vertical axis and the direction of the incident beam. Corresponding values  $c_L = 0.99$  (1), 0.95 (2), 0.92 (3), and 0.8 (4).

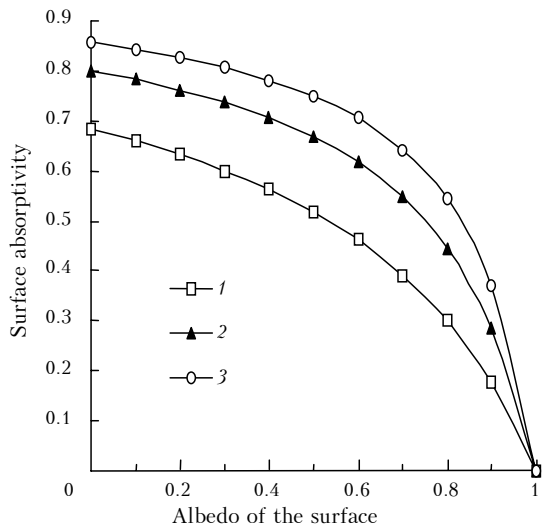


**Fig. 3.** The fraction of absorbed radiation as a function of the underlying surface albedo in snowfall:  $\sigma_{SN} = 0$  (1);  $5$  (2);  $10 \text{ km}^{-1}$  (3). Other parameters of the model:  $H = 1$  km,  $\sigma_{CL} = 20 \text{ km}^{-1}$ .

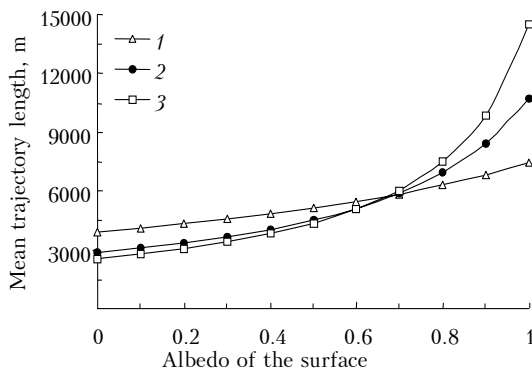


**Fig. 4.** Mean length of the photon trajectory in the medium as a function of the underlying surface albedo for  $\sigma_{SN} = 0$  (1);  $5$  (2);  $10 \text{ km}^{-1}$  (3). Other parameters of the model:  $H = 1$  km,  $\sigma_{CL} = 20 \text{ km}^{-1}$ .

## 2. Model with a point source

As for the model with a point source, we were interested in illumination of the underlying surface  $\Phi(r)$  (Fig. 5) and the radial distribution of the power of the radiant flux incident on the surface  $F(r) = 2\pi r\Phi(r)$  (Fig. 6) as functions of the distance to the source  $r$ .

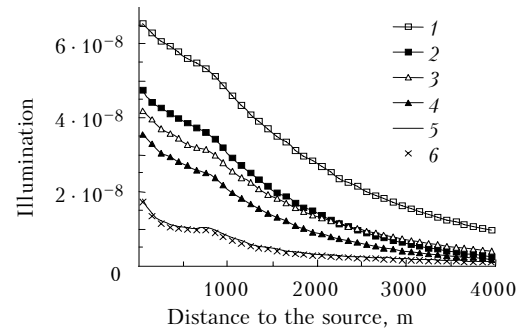


**Fig. 5.** Illumination of the surface ( $\text{W}/\text{m}^2$ ) as a function of distance to the source (of unit power) for  $H = 1$  km and  $Q = 1$  (1),  $H = 1$  km and  $Q = 0$  (2),  $H = 0.4$  km and  $Q = 1$  (3),  $H = 0.4$  km and  $Q = 0$  (4),  $H = 0.1$  km and  $Q = 1$  (5),  $H = 0.1$  km and  $Q = 0$  (6).

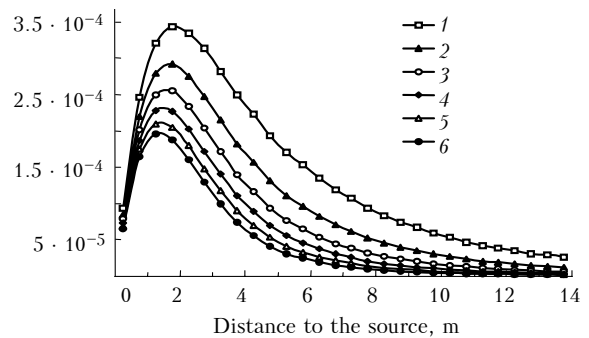


**Fig. 6.** Radial distribution of the flux power  $F(r) = 2\pi r\Phi(r)$  ( $\text{W}/\text{m}^2$ ), where  $\Phi(r)$  is the illumination of the underlying surface at the distance  $r$  from the source for different values of the underlying surface albedo:  $Q = 1$  (1); 0.8 (2); 0.6 (3); 0.4 (4); 0.2 (5); 0 (6). The parameter  $r$  is plotted along the abscissa in meters. Other parameters of the model:  $h = 1$  km,  $H = 1$  km,  $\sigma_{CL} = 20 \text{ km}^{-1}$ ,  $\sigma_{SN} = 0 \text{ km}^{-1}$ .

The power of the point source in Figs. 5 and 6 was taken to be equal to 1,  $\sigma_{SN} = 0$ , and the distance to the lower boundary of cloudiness  $h$  was set equal to 1 km. Note the presence of inflection in the curves of the illumination as a function of distance to the source (see Fig. 5). In particular, the plots in Figs. 5 and 6 show that the illumination of the underlying surface at a distance of about 1 km from the point source with a power of several kilowatts under cloudy conditions can be close to that formed by a half moon at zenith ( $\approx 0.03 \text{ lux}$ ). The illumination plots for snowfall conditions have a significantly sharper peak at zero (Fig. 7).

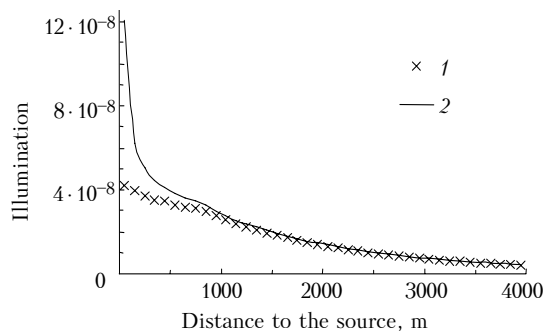


**Fig. 7.** Illumination of the underlying surface ( $\text{W}/\text{m}^2$ ) as a function of the distance to a source with unit power for  $\sigma_{\text{SN}} = 0$  (1) and  $0.1 \text{ km}^{-1}$  (2). Other parameters of the model:  $H = 0.4 \text{ km}$ ,  $h = 1 \text{ km}$ ,  $Q = 1$ .

### 3. On the influence of inhomogeneous cloudiness on the directional diagram of the radiation returning to the surface

Alongside the simplest model of stratus cloudiness (homogeneous layer bounded by two parallel planes), the Gaussian geometrical model of cumulus cloudiness was used in the numerical experiment (see Ref. 4). The cumulus clouds were assumed to be purely scattering with extinction coefficient  $\sigma_{\text{CL}} = 50 \text{ km}^{-1}$  and the same scattering phase function ( $C_1$  cloud model) as was used for the stratus model. The parameters of the cumulus cloudiness (cloud fraction  $N_0$ , characteristic diameter  $D_0$ , and mean height of clouds  $H_0$ ) were selected so that the probability  $B$  of the photon returning from the cloudy layer downwards coincides with the corresponding probability for a stratus cloud with the parameters  $H = 200 \text{ m}$  and  $\sigma_{\text{CL}} = 20 \text{ km}^{-1}$  ( $B = 0.32$ ). The directional diagrams of radiation returning from the cloudy layer downwards for a stratus cloud and cumulus cloudiness with  $N_0 = 0.5$ ,  $D_0 = 1 \text{ km}$ , and  $H_0 = 0.7 \text{ km}$  are plotted in Fig. 8.

The directional diagram of the cumulus cloudiness is taken to mean, of course, the directional diagram averaged over the horizontal plane. Note that the value  $c_{\perp}$  for cumulus cloudiness is a bit greater than for stratus. The probability of photon return for the set of cumulus cloudiness parameters  $N_0 = 0.5$ ,  $D_0 = 0.2 \text{ km}$ , and  $H_0 = 0.43 \text{ km}$  is also approximately equal to 0.32, but the directional diagram practically coincides with the directional diagram for the stratus cloud model.

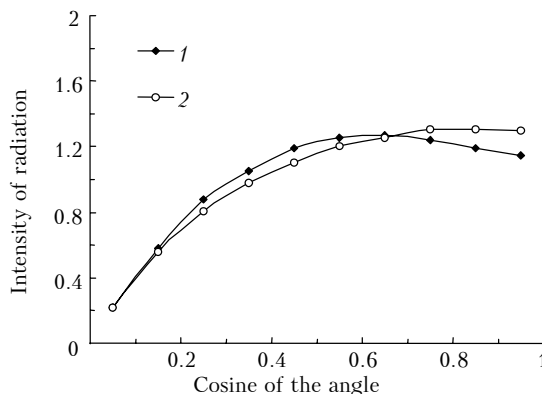


**Fig. 8.** Directional diagram of the radiation returning to the underlying surface for stratus cloudiness (1) with  $H = 0.2 \text{ km}$ ,  $\sigma_{\text{CL}} = 20 \text{ km}^{-1}$ , and for cumulus cloudiness (2) with  $H_0 = 0.7 \text{ km}$ ,  $\sigma_{\text{CL}} = 50 \text{ km}^{-1}$ ,  $N_0 = 0.5$ ,  $D_0 = 1 \text{ km}$ . The dependence presented here is that of the radiation intensity on the cosine of the angle between the vertical axis and the direction of the incident beam. Corresponding values  $c_{\perp} = 0.86$  (1) and  $0.89$  (2).

We note in conclusion that the effect caused by multiple re-reflection of radiation between the underlying surface and the atmospheric layer for the model with a plane-parallel source at the upper boundary of the atmosphere were investigated in Ref. 5. In particular, authors of Ref. 5 concluded that the presence of a thin cloudy layer can lead to such effects as an increase in the mean intensity of solar radiation near the underlying surface and a decrease in the albedo of the system atmosphere – underlying surface.

#### Acknowledgment

The work was supported in part by Russian Foundation for Basic Research (Grants No. 98–01–00685, No. 00–01–00797, and No. 00–05–65456) and INTAS (Grant No. IR–97–1441).

#### References

1. D. Deirmendjian, *Electromagnetic Scattering on Spherical Polydispersions* (American Elsevier, New York, 1969).
2. A.G. Borovoi, N.A. Vostretsov, A.F. Zhukov, et al., *Atmos. Oceanic Opt.* **10**, No. 3, 141–145 (1997).
3. A.F. Zhukov, *Atmos. Oceanic Opt.* **6**, No. 1, 19–21 (1993).
4. S.M. Prigarin, B.A. Kargin, and U.G. Oppel, *Pure and Applied Optics*. **A. 7**, No. 6, 1389–1402 (1998).
5. S.M. Prigarin and U.G. Oppel, *Pure and Applied Optics*. **A. 7**, No. 6, L79–L83 (1998).